

Disappearance and recovery of colossal permittivity in (Nb+Mn) co-doped TiO₂

Chao Yang¹, Xianhua Wei^{1*}, Jianhua Hao^{2**}

¹*State Key Laboratory of Environmental Friendly Energy Materials, Southwest University of Science and Technology, Mianyang 621010, P. R. China*

²*Department of Applied Physics, The Hong Kong Polytechnic University, Hung Hom, Hong Kong, P. R. China*

Abstract: We investigate the effects of doping and annealing on the dielectric properties of metal ion-doped TiO₂ ceramics. Colossal permittivity (CP) above 10⁴ was observed for single Nb ion doped TiO₂, which was dominated by electron transport related interfacial polarization. Moreover, the CP can be dropped to about 100 when simultaneously introducing Mn ion into the sample. The disappearance of CP behaviors might be due to the multivalence of Mn which would inhibit the reduction of Ti⁴⁺ to Ti³⁺, and thus reduce delocalized electrons. Interestingly, the CP behavior was recovered for the (Nb+Mn) co-doped TiO₂ when post-sintering in N₂ atmosphere. The recovery of CP in the sample after annealing can be ascribed to the semiconducting grain and the insulating grain boundary, according to impedance spectroscopy. The results are helpful for further understanding the CP mechanism and exploring an approach to tune CP behavior reversibly.

Keywords: Colossal permittivity, Mn-Doped TiO₂, Impedance spectroscopy, XPS, annealing

*Corresponding author, weixianhua@swust.edu.cn (X. H. Wei)

** Corresponding author, jh.hao@polyu.edu.hk (J. H. Hao).

1. Introduction

Colossal permittivity (CP) ($\epsilon_r > 10^4$) and low loss (mostly < 0.05) were found in metal ion co-doped rutile TiO₂ ceramics by Liu's group.¹ The dielectric properties are almost independent over a wide frequency and temperature range, which is superior to previously studied CP materials, such as ferroelectrics,² CaCu₃Ti₄O₁₂ (CCTO),^{3,4} doped NiO,⁵ and La_{15/8}Sr_{1/8}NiO₄.⁶ Therefore, the CP properties based on co-doped TiO₂ have attracted considerable attention due to its potential applications in high-performance capacitors, miniaturized electronics and high-density energy storage. Effects of doped elements on the dielectric properties of TiO₂ and the origin of their CP are the two concerns which would play a vital role in practical application of the CP materials. Generally, donor doping in TiO₂ is considered to raise the permittivity due to the creation of delocalized electrons by reducing Ti⁴⁺ to Ti³⁺. Meanwhile, acceptor doping lowers the dielectric losses because it is regarded as providing a local oxygen-deficient environment to hold back the delocalized electrons, according to the formation of electron-pinned defect-dipole (EPDD). Up to now, CP behaviors have been confirmed in TiO₂ ceramics by co-doping acceptor ions (trivalent ions: Al, Ga, In, or rare earth ions; bivalent ions: Zn, or alkaline earth ions) or isovalent ion (Zr) and donor elements (pentavalent ions: Nb or Ta).⁷⁻²¹ However, the mechanism is still not fully understood. Other mechanisms have also been presented except for EPDD, including interface effect caused by internal barrier layer capacitor (IBLC) effect,^{10,22} the electrode effect,¹¹ hopping conductivity,²³ surface barrier layer effect,²⁴ as well as microscopic inhomogeneities and polaronic relaxation.²⁵ Those explanations might be relevant to different synthesis processes or combination of co-

doped ions.

Manganese (Mn) has been widely used as doping element for the ceramic capacitors. Its doping into perovskite oxide like (Ba, Sr)TiO₃,²⁶ Ba(Zr, Ti)O₃²⁷ has shown positive effects in reducing the dielectric loss, and enhancing the dielectric constant. It could be mainly attributed to the decrease in electron concentration and oxygen vacancies and the reorientation of the defect complex. By contrast, Mn doping can suppress the dielectric permittivity in CCTO by up to two orders of magnitude.²⁸ The observation was explained by the decrease of potential barrier height at the grain boundary and charge compensation for the conduction electrons caused by the Mn doping.²⁸ However, Mn-doped CP TiO₂ ceramic has not yet been reported. Therefore, it would be quite intriguing to investigate the Mn doping effect on the dielectric properties of TiO₂ with different possible mechanisms. In this work, the disappearance of the CP is found in the as-fabricated (Nb+Mn) co-doped TiO₂ ceramics. It is intriguing that the CP can be recovered by annealing the ceramics in N₂ atmosphere, showing reversible switching of CP which has not yet been found. The relative mechanisms are discussed based on defect dipole and IBLC effect.

2. Experimental procedure

(Nb+Mn) co-doped TiO₂ ceramics were prepared by a conventional solid state reaction method. The starting raw materials contain rutile TiO₂ (99.99%), Nb₂O₅ (99.99%) and MnO (99.99%). These powders were weighted according to a composition of (Nb_{0.5}Mn_{0.5})_xTi_{1-x}O₂ ($x = 0.25\%$, 0.5% , 1% , 2%) and then milled by ball-milling with ZrO₂

balls for 6 h ~ 8 h in ethanol. The mixed slurry was heated to evaporate ethanol. Then the dry powders were calcined at 1000 °C for 4 h in air with a heating rate of 3 °C/min. After this pre-sintering process, the samples were reground and the dried powders were pressed into pellets by uniaxial compression. These ceramic biscuits with a diameter of 10 mm and a thickness of 1.5 mm were fired at 650 °C for 6 h in air to remove the organic polyvinyl alcohol binder. Finally, the samples were sintered at 1400 °C for 10 h by heating rate of 3°C/min and then cooled down to room temperature. In addition, the doping level of $x = 2\%$ sample was post-sintered at 1400 °C for 5 h in N₂ atmosphere. The phase of co-doped TiO₂ ceramics was confirmed using an X-ray diffraction technique (XRD, DMAX1400, Rigaku), and Raman spectroscopy (InVia, Renishaw) excited by 514 nm laser line. The microstructures and elemental mapping of the samples were characterized using scanning electron microscopy (SEM, MAIA3, Tescan). X-ray photoelectron spectroscopy (XPS) was used to analyze the valence states of elements in the ceramics. A monochromatic aluminium K α radiation source with energy of 1486.8 eV was used in Thermo SCIENTIFIC ESCALAB 250Xi system (Escalab 250Xi; Thermo Scientific, Leicestershire, UK). Room temperature dielectric properties and the impedance spectroscopy were measured using a Partulab HDMS-1000 high-temperature dielectric measurement system (Wuhan Partulab Technology Co. Ltd, China) combined with an Agilent 4294A Precision Impedance Analyzer (Agilent Technologies Inc., USA).

3. Results and discussion

Fig. 1 shows the XRD patterns of all sintered (Nb_{0.5}Mn_{0.5})_xTi_{1-x}O₂ ceramics in the

2θ range of 20° to 75° . The diffraction peaks of all samples can be indexed to the rutile TiO_2 (JCPDS 21-1276). No peaks of secondary phases were observed in the XRD patterns and all samples exhibit a rutile phase structure, indicating Nb and Mn elements have incorporated into the TiO_2 lattices to form homogenous solid solutions. Generally, the presence of secondary phases is not beneficial to the dielectric property, which has been confirmed in the (Bi+Nb) co-doped TiO_2 and other microwave dielectric materials system.^{7,29} Therefore, a small amount of Mn ions was doped into TiO_2 in order to exclude the impact of secondary phase in colossal permittivity. The Raman spectra of the sintered (Nb+Mn) co-doped TiO_2 ceramics were recorded in the range of $100 \sim 1000 \text{ cm}^{-1}$, as shown in Fig. 2. Four Raman active fundamentals were found in these samples, corresponding to B_{1g} (143 cm^{-1}), E_g (447 cm^{-1}), A_{1g} (612 cm^{-1}), and B_{2g} (826 cm^{-1}), respectively.⁷ It is further confirmed that the existence of the rutile phase because of the appearance of B_{1g} , E_g and A_{1g} modes in all compositions. Besides, the 239 cm^{-1} peak is obviously visible in the samples, which is a multi-phonon peak for second-order effect.³⁰ The peak is closely related to the internal stress and partial reduction in the TiO_2 grains caused by doping elements with different radii into the host lattice. Thus, the results of Raman suggest the pure rutile TiO_2 of the doped ceramics, which is compatible with the analysis of XRD patterns.

The SEM micrographs of our sintered ceramic samples are shown in Figs. 3(a) ~ (f). For the ceramics of (Nb+Mn) co-doping, the grains with an obvious bimodal distribution are tightly arranged. Both larger coarse grains and smaller ones exhibit a gradual decrease with the increasing doping constants from 0.25% to 2%. However, the grains grow

significantly after re-sintering them in N₂ atmosphere. Typically, for the doping level of 2%, the size of larger coarse grains is doubled to around 40 μm while that of smaller ones is almost tripled to about 20 μm. Normally, the grain growth is related to the liquid phase sintering mechanism, which means the mass transport across the grain boundary by diffusion of ions or atoms.³¹ For the co-doped TiO₂ ceramics herein, the doping Mn elements might inhibit the grain boundary movement, and resulting in the decrease of grain size.³² However, the different sintering atmosphere can give rise to the disparity of grain size at the same temperature.³³ The grain for the sample grows larger after sintering in N₂, which is similar to the Ba doped Sr_{0.97}Sm_{0.02}TiO₃ ceramics.³³ To further characterize the elemental composition and distributions, the element mapping of (Nb+Mn) co-doped TiO₂ is conducted, as presented in Fig. 4. It can be seen that the elements of Nb, Mn, Ti, and O are homogeneously distributed across the grains and grain boundaries before and after annealing in N₂ atmosphere. This result indicates no second phase in our co-doped TiO₂ ceramics, which is coincident with the XRD and Raman results.

As shown in the Fig. 5, the dielectric properties of (Nb+Mn) co-doped TiO₂ ceramics with different compositions are measured at frequencies ranging from 100 Hz to 1 MHz. It is widely accepted that TiO₂ have the largest dielectric constant among the single oxides and it can also improve the permittivity by adding it into other dielectric ceramics.^{1, 34} **Singly** doping Nb can significantly increase the permittivity (beyond 10⁴) of the host TiO₂. It is generally accepted that it can be attributed to a typical interfacial polarization effect that space charges accumulating at grain boundaries.¹ Thus, it shows a very large

dielectric loss. Besides, co-doping with fixed valence acceptor elements (e.g., Mg, Zn, Al, and In) has no significant effect on the permittivity of TiO₂, but reduces the dielectric loss on the condition that the charge balance is kept, according to EPDD mechanism. Unfortunately, the dielectric permittivity drastically drops to 100 ~ 200 while co-doping with Mn and Nb, even at the lowest doping level of 0.25%. The similar phenomenon was previously observed in Mn doped CCTO, which is ascribed to the suppression of bulk semiconductivity of CCTO.²⁸ In addition, the CP would also disappear in (Nb+Al) co-doped TiO₂ if the amount of Al-doping exceeds Nb.¹⁰ The disappearance of CP in this work may be closely related to the multivalence of Mn. Interestingly, the CP (~39680, 1 kHz) is achieved again in (Nb+Mn) co-doped TiO₂ by post-sintering the sample at 1400 °C for 5 hrs in N₂ atmosphere. The corresponding dielectric loss is about 0.1 at 1 kHz, which is shown in the inset of Fig. 5.

The fascinating phenomenon of reversible CP tuning makes us further to investigate the potential mechanism. Firstly, XPS analysis was carried out to explain the changes of CP. The Mn elements are not detected in the XPS of $x = 2\%$ (0.58 at%) sample. It is possible that the contents of Mn element are too low to detected, which is similar to the Mn doped Ti_{1-x}Cu_{x/3}Nb_{2x/3}O₂ ceramics at the Mn doping level of 0.6 at%.³⁵ As shown in Fig. 6, we compare the XPS results of Ti and O elements between those samples of Nb-only (with CP), $x = 2\%$ (without CP) and $x = 2\%$ after post-sintering (with CP). From the XPS results in Fig. 6(a, b, c), three components of O 1s peaks can be observed, including ~529.5 eV for bulk Ti-O, ~530.9 eV associated with oxygen vacancies, and 531.9 eV for adsorbed surface H₂O. The oxygen vacancy concentration for the three samples can be

computed to be 20.36%, 22.17% and 23.5%, respectively. It is easy to understand the increasing of oxygen vacancy concentration. The introduction of acceptor element into Ti site can cause oxygen vacancies for charge compensation as: $\text{MnO} \xrightarrow{\text{TiO}_2} \text{Mn}_{\text{Ti}}'' + \text{V}_{\text{O}}'' + \text{O}_{\text{O}}$. Moreover, it is commonly believed that the post sintering of sample in N_2 atmosphere can provide an oxygen-deficient environment and increase the concentration of oxygen vacancy in the ceramic. In addition, Ti^{4+} and Ti^{3+} signals can be detected as present in Fig. 6(d, e, f). Two obvious peaks of the Ti 2p with 2p_{3/2} and 2p_{1/2} can be observed at binding energies of 458.5 eV and 464.2 eV, respectively, corresponding to Ti^{4+} . The other two small peaks locating at 457.2 eV and 462.4 eV prove the existence of Ti^{3+} . The percentages of $\text{Ti}^{3+}/\text{Ti}^{4+}$ in the three samples can be calculated to be 3.7%, 2.7%, and 3.8%, respectively. The reduction process of Ti^{4+} to Ti^{3+} can be explained by the introduction of Nb^{5+} as: $\text{Nb}_2\text{O}_5 + 2\text{TiO}_2 \xrightarrow{4\text{TiO}_2} 2\text{Nb}_{\text{Ti}}^{\bullet} + 2\text{Ti}_{\text{Ti}}' + 8\text{O}_{\text{O}} + 1/2\text{O}_2$ and $\text{Ti}^{4+} + \text{e} \rightarrow \text{Ti}^{3+}$. However, there is an obvious decrease in the proportion of Ti^{3+} when the Mn element is doped into Ti position. It is well known that manganese oxide is an additive for valence compensation and vacancy suppression of titanate, niobate and other oxides.^{36, 37} For example, Mn^{2+} doping is effective to suppress the transition of Cu^{2+} to Cu^+ of $\text{Ti}_{1-x}\text{Cu}_{x/3}\text{Nb}_{2x/3}\text{O}_2$ ceramics.³⁵ Similarly, we can speculate that the introduction of Mn could inhibit the reduction process of Ti^{4+} to Ti^{3+} in our samples. It is possible that some of the Mn^{2+} can first oxidize to the trivalent state and subsequently enter the Ti sites during sintering in air. Besides, the transformation of Mn^{3+} to Mn^{2+} is prior to the conversion of Ti^{4+} to Ti^{3+} .³⁸ In other words, the delocalized electrons created by Nb doping would be reduced due to the co-doping of multivalent Mn. Noted that the contents of Ti^{3+} for the

same sample increase after the post sintering in N₂ atmosphere. In such reducing atmosphere, the valence compensation and vacancy suppression of Mn doping is weakened. It also can be explained that the Mn doped in Ti site changes its valence from +4 to +3 to +2 with the decrease of the oxygen activity in the surroundings.³⁹ Therefore, more delocalized electrons could be recovered, which at last results in the appearance of CP.

Moreover, the complex impedance spectra (Cole-Cole plot) technique was used to analyze the relation between microstructure and electrical properties. As shown in Fig. 7, we measured the high temperature complex impedance (170 °C ~ 380 °C) for $x = 2\%$ sample before and after the post-sintering in N₂ atmosphere. In Fig. 7A, the semi-arcs can be clearly observed at different temperature. The complete small arcs in high frequency and tails in low frequency represent the grain arc and grain boundary arc, respectively. Furthermore, the resistances of the grain and grain boundary significantly decreased with increasing temperature, which manifests that the resistances are thermally activated and the conductivity σ may obey the Arrhenius law: $\sigma_{dc} = \sigma_0 \exp(-E_a / k_B T)$, where σ_0 is a constant value, E_a is the activation energy, k_B is the Boltzmann constant, and T is the absolute temperature.⁴⁰ For example, the resistance of the grain (106370 Ω) and grain boundary (843630 Ω) can be simulated from the impedance spectrum arc at 170 °C for the sample with $x = 2\%$. The conductive active energies of grain and grain boundary are well fitted as present in Fig. 7B. The E_g (active energy of grain) value is 0.79 eV, being analogous to that of (In+ Nb) co-doped TiO₂.¹ Meanwhile, the E_{gb} (active energy of grain boundary) value is calculated to be 0.86 eV, which is close to the E_g . According to the

IBLC effect, it is a significant feature for a large difference between grain and grain boundary activation energy. Therefore, we can speculate that the IBLC effect doesn't work in (Nb+Mn) co-doped TiO₂ without CP behavior. Comparatively speaking, the resistance of the grain and grain boundary decreases sharply for the sample after the post-treatment process in N₂ atmosphere. Firstly, it can be seen from the enlargement zone at high frequency in the inset of Fig. 7C that the semicircular arc shows a nonzero intercept which represents the grain resistance. It is accepted that the decreased resistance of grains can be attributed to the increase of Ti³⁺ ions content based on the XPS results, which is similar to the (Nb+In) co-doped TiO₂.⁴⁰ Besides, the oxygen vacancy concentration increased after annealing in nitrogen atmosphere, resulting in a low resistance of grain boundary. But it is still far larger than grain resistance. Meanwhile, the corresponding E_{gb} (0.82 eV) shows a little diminution. The increasing of oxygen vacancy strengthens their own correlation and thus improves the migration of oxygen vacancies, leading to the decrease in activation energy.⁴¹ Therefore, it can be concluded that the IBLC effect should be the dominant mechanism of the recovery of the CP in our annealed ceramic.

4. Conclusions

In this work, we observed the effect of variable valence Mn ion on the CP properties of Nb doped TiO₂ ceramics. It is remarkable that the CP drops dramatically even if the doping concentration of Mn is very low. The results can be understood that the introduction of variable valence acceptor can inhibit the reduction of Ti⁴⁺ to Ti³⁺. The delocalized electrons are fully compensated by acceptor Mn-doping, which results in a

small permittivity. Interestingly, the CP is tunable and recovered for the (Mn+Nb) co-doped TiO₂ sample after the heat-treatment in N₂ atmosphere. It can be explained that the variation of Mn valence can be restrained in the oxygen-deficient environment and thus a small amount uncompensated electrons can bring about the colossal dielectric constant. This work would provide a guidance to further researching the CP materials by incorporating into variable valence elements and developing tunable CP devices.

Acknowledgment

This work has been supported by the Program for Young Science and Technology Innovation Team of Sichuan Province (2017TD0020). J. H. acknowledges financial support from the grant of Research Grants Council of Hong Kong (GRF No. PolyU 153004/14P).

References

- [1] W. B. Hu, Y. Liu, R. L. Withers, T. J. Frankcombe, L. Norén, A. Snashall, M. Kitchin, P. Smith, B. Gong, H. Chen, J. Schiemer, F. Brink, and J. Wong-Leung, Electron-pinned defect-dipoles for high-performance colossal permittivity materials, *Nature Mater.* 12 (2013) 821-826.
- [2] M. T. Buscaglia, M. Viviani, V. Buscaglia, L. Mitoseriu, A. Testino, P. Nanni, Z. Zhao, M. Nygren, C. Harnagea, D. Piazza, and C. Galassi, High dielectric constant and frozen macroscopic polarization in dense nanocrystalline BaTiO₃ ceramics, *Phys. Rev. B* 73 (2006) 064114.
- [3] T. T. Fang, H. K. Shiau. Mechanism for developing the boundary barrier layers of CaCu₃Ti₄O₁₂. *J. Am. Ceram. Soc.* 87 (2004) 2072-2079.
- [4] C. C. Homes, T. Vogt, S. M. Shapiro, S. Wakimoto, and A. P. Ramirez, Optical response of high-dielectric-constant perovskite-related oxide, *Science* 293 (2001) 673-676.
- [5] J. B. Wu, C. W. Nan, Y. H. Lin, and Y. Deng, Giant dielectric permittivity observed in Li and Ti doped NiO, *Phys. Rev. Lett.* 89 (2002) 217601.
- [6] S. Krohns, P. Lunkenheimer, Ch. Kant, A. V. Pronin, H. B. Brom, A. A. Nugroho, M. Diantoro, and A. Loidl, Colossal dielectric constant up to gigahertz at room temperature, *Appl. Phys. Lett.* 94 (2009) 122903.
- [7] X. J. Cheng, Z. W. Li, and J. G. Wu, Colossal permittivity in ceramics of TiO₂ Co-doped with niobium and trivalent cation, *J. Mater. Chem. A* 3 (2015) 5805-5810.
- [8] Z. W. Li, J. G. Wu, D. Q. Xiao, J. G. Zhu, W. J. Wu, Colossal permittivity in titanium

dioxide ceramics modified by tantalum and trivalent elements, *Acta Mater.* 103 (2016) 243-251.

[9] W. Tuichai, P. Srepusharawoot, E. Swatsitang, S. Danwittayakuld, and P. Thongbai, Giant dielectric permittivity and electronic structure in (Al+Sb) co-doped TiO₂ ceramics, *Microelectron. Eng.* 146 (2015) 32-37.

[10] Y. L. Song, X. J. Wang, X. Q. Zhang, Y. Sui, Y. Zhang, Z. G. Liu, Z. Lv, Y. Wang, P. Xu, and B. Song, The contribution of doped-Al on the colossal permittivity properties of Al_xNb_{0.03}Ti_{0.97-x}O₂ rutile ceramics, *J. Mater. Chem. C* 4 (2016) 6798-6805.

[11] W. Dong, W. B. Hu, A. Berlie, K. Lau, H. Chen, R. L. Withers, and Y. Liu, Colossal dielectric behavior of Ga+Nb co-doped rutile TiO₂, *ACS Appl. Mater. Interfaces* 7 (2015) 25321-25325.

[12] W. B. Hu, K. Lau, Y. Liu, R. L. Withers, H. Chen, L. Fu, B. Gong, and W. Hutchison, Colossal dielectric permittivity in (Nb+Al) codoped rutile TiO₂ ceramics: compositional gradient and local structure, *Chem. Mater.* 27 (2015) 4934-4942.

[13] M. Y. Tse, M. K. Tsang, Y. T. Wong, Y. L. Chan, and J. H. Hao, Simultaneous observation of up/down conversion photoluminescence and colossal permittivity properties in (Er+Nb) co-doped TiO₂ materials, *Appl. Phys. Lett.* 109 (2016) 042903.

[14] M. Y. Tse, X. H. Wei, and J. H. Hao, High-performance colossal permittivity materials of (Nb+Er) co-doped TiO₂ for large capacitors and high-energy-density storage devices, *Phys. Chem. Chem. Phys.* 18 (2016) 24270-24277.

[15] Z. W. Li, J. G. Wu, and W. J. Wu, Composition dependence of colossal permittivity in (Sm_{0.5}Ta_{0.5})_xTi_{1-x}O₂ ceramics, *J. Mater. Chem. C* 3 (2015) 9206-9216.

- [16] X. H. Wei, W. J. Jie, Z. B. Yang, F. G. Zheng, H. Z. Zeng, Y. Liu, and J. H. Hao, Colossal permittivity properties of Zn, Nb co-doped TiO₂ with different phase structures, *J. Mater. Chem. C* 3 (2015) 11005-11010.
- [17] W. Dong, W. B. Hu, T. Frankcombe, D. H. Chen, C. Zhou, Z. X. Fu, L. Cândido, G. Q. Hai, H. Chen, Y. X. Li, R. Withers and Y. Liu, Colossal permittivity with ultralow dielectric loss in In+Ta co-doped rutile TiO₂, *J. Mater. Chem. A* 5 (2017) 5436-5441.
- [18] C. Yang, M. Y. Tse, X. H. Wei, J. H. Hao, Colossal permittivity of (Mg+Nb) co-doped TiO₂ ceramics with low dielectric loss, *J. Mater. Chem. C* 5 (2017) 5170-5175.
- [19] X. G. Zhao, P. Liu, Dielectric and electric relaxations induced by the complex defect clusters in (Yb+Nb) co-doped rutile TiO₂ ceramics, *J. Am. Ceram. Soc.* 100 (2017) 3505-3513.
- [20] Z. W. Li, X. Luo, W. J. Wu, J. G. Wu, Niobium and divalent-modified titanium dioxide ceramics: colossal permittivity and composition design, *J. Am. Ceram. Soc.* 100 (2017) 3004-3012.
- [21] T. Nachaithong, W. Tuichai, P. Kidkhunthod, N. Chanlek, P. Thongbai, S. Maensiri, Preparation, characterization, and giant dielectric permittivity of (Y³⁺ and Nb⁵⁺) co-doped TiO₂ ceramics, *J. Eur. Ceram. Soc.* 37 (2017) 3521-3526.
- [22] J. L. Li, F. Li, C. Li, G. Yang, Z. Xu, S. J. Zhang, Evidences of grain boundary capacitance effect on the colossal dielectric permittivity in (Nb+In) co-doped TiO₂ ceramics, *Sci. Rep.* 5 (2015) 8295.
- [23] X. G. Zhao, P. Liu, Y. C. Song, A. P. Zhang, X. M. Chen, J. P. Zhou, Origin of colossal permittivity in (In_{1/2}Nb_{1/2})TiO₂ via broadband dielectric spectroscopy, *Phys Chem. Chem.*

Phys. 17 (2015) 23132.

[24] T. Nachaithong, P. Kidkhunthod, P. Thongbai, S. Maensiri, Surface barrier layer effect in (In+ Nb) co-doped TiO₂ ceramics: an alternative route to design low dielectric loss, J. Am. Ceram. Soc. 100 (2017) 1452-1459.

[25] S. Mandal, S. Pal, A. K. Kundu, K. S. R. Menon, A. Hazarika, M. Rioult, and R. Belkhou, Direct view at colossal permittivity in donor-acceptor (Nb, In) co-doped rutile TiO₂, Appl. Phys. Lett. 109 (2016) 092906.

[26] T. Hu, T. J. Price, D. M. Iddles, A. Uusimäki, H. Jantunena, The effect of Mn on the microstructure and properties of BaSrTiO₃ with B₂O₃-Li₂CO₃, J. Eur. Ceram. Soc. 25 (2005) 2531-2535.

[27] W. Cai, C. L. Fu, J. C. Gao, X. L. Deng, Effect of Mn doping on the dielectric properties of BaZr_{0.2}Ti_{0.8}O₃ ceramics, J. Mater. Sci: Mater. Electron. 21 (2010) 317-325.

[28] J. Cai, Y. H. Lin, B. Cheng, C. W. Nan, Dielectric and nonlinear electrical behaviors observed in Mn-doped CaCu₃Ti₄O₁₂ ceramic, Appl. Phys. Lett. 91 (2007) 252905.

[29] H. Y. Yang, E. Z. Li, H. C. Yang, H. C. He, R. S. Zhang, Synthesis of Zn_{0.5}Ti_{0.5}NbO₄ microwave dielectric ceramics with Li₂O-B₂O₃-SiO₂ glass for LTCC application, Int. J. Appl. Glass. Sci. (2017), DOI: 10.1111/ijag.12334.

[29] V. Swamy, B. C. Muddle, Q. Dai, Size-dependent modifications of the Raman spectrum of rutile TiO₂, Appl. Phys. Lett. 89 (2006) 163118.

[30] W. Tuichai, P. Srepusharawoot, E. Swatsitang, S. Danwittayakuld, P. Thongbai, Giant dielectric permittivity and electronic structure in (Al+ Sb) co-doped TiO₂ ceramics, Microelectron. Eng. 146 (2015) 32-37.

- [31] B. Zhang, Q. Zhao, A. M. Chang, H. T. Ye, S. Chen, Y. Q. Wu, New negative temperature coefficient thermistor ceramics in Mn-doped $\text{CaCu}_{3-x}\text{Mn}_x\text{Ti}_4\text{O}_{12}$ ($0 \leq x \leq 1$) system, *Ceram. Inter.* 40 (2014) 11221-11227.
- [32] G. Y. Li, H. X. Liu, H. Hao, J. J. Liu, Z. Chen, X. D. Huang, M. H. Cao, Z. H. Yao, Dielectric properties and relaxation behaviors of Ba doped $\text{Sr}_{0.97}\text{Sm}_{0.02}\text{TiO}_3$ ceramics in different sintering atmospheres, *Ceram. Inter.* 42 (2016) 16782–16788.
- [33] H. Y. Yang, E. Z. Li, Y. F. Yang, Y. Shi, H. C. He, S. R. Zhang, Co_2O_3 substitution effects on the structure and microwave dielectric properties of low-firing $(\text{Zn}_{0.9}\text{Mg}_{0.1})\text{TiO}_3$ ceramics, *Ceram. Inter.* (2017), <https://doi.org/10.1016/j.ceramint.2017.12.097>.
- [34] H. Shao, Z. Liu, G. Jian, M. S. Ma, Y. X. Li, Effects of Mn^{2+} doping on the microwave dielectric properties of $\text{Ti}_{1-x}\text{Cu}_{x/3}\text{Nb}_{2x/3}\text{O}_2$ ceramics, *Ceram. Int.* 43 (2017) 13895-13900.
- [35] H. I. Hsiang, S. H. Chung, Effects of B_2O_3 addition on the microstructure and microwave dielectric properties of $\text{La}_4\text{Ba}_2\text{Ti}_5\text{O}_{18}$, *J. Alloy. Compd.* 465 (2008) 356–360.
- [36] F. Dogan, S. Chao, Effects of manganese doping on the dielectric properties of titanium dioxide ceramics, *J. Am. Ceram. Soc.* 94 (2011) 179–186.
- [37] J. H. Moon, H. M. Jang, Effects of Sintering Atmosphere on Densification Behavior and Piezoelectric Properties of $\text{Pb}(\text{Ni}_{1/3}\text{Nb}_{2/3})\text{O}_3\text{-PbTiO}_3\text{-PbZrO}_3$ Ceramics, *J. Am. Ceram. Soc.* 76 (1993) 549-552.
- [38] H.I. Yoo, T. S. Oh, H. S. Kwon, D. K. Shin, J. S. Lee, Electrical conductivity-defect structure correlation of variable-valence and fixed-valence acceptor-doped BaTiO_3 in quenched state, *Phys. Chem. Chem. Phys.* 11 (2009) 3115-3126.

[39] J. L. Li, F. Li, Y. Y. Zhuang, L. Jin, L. H. Wang, X. Y. Wei, Z. Xu, and S. J. Zhang, Microstructure and dielectric properties of (Nb+ In) co-doped rutile TiO₂ ceramics, J. Appl. Phys. 116 (2014) 074105.

[40] X. F. Wang, X. M. Lu, C. Zhang, X. B. Wu, W. Cai, S. Peng, H. F. Bo, Y. Kan, F. Z. Huang, J. S. Zhu, Oxygen-vacancy-related high temperature dielectric relaxation in SrTiO₃ ceramics, J. Appl. Phys. 107 (2010) 114101.

Figure captions

FIG. 1. XRD patterns of 1% only Nb-doped TiO₂(NTO), (Nb_{0.5}Mn_{0.5})_xTi_{1-x}O₂ (NMTO, $x = 0.25\%$, 0.5% , 1% , 2%), and $x = 2\%$ after post-sintering in N₂ ceramics.

FIG. 2. Raman spectra of pure TiO₂, 1% only Nb-doped TiO₂, (Mn_{0.5}Nb_{0.5})_xTi_{1-x}O₂ ($x = 0.25\%$, 0.5% , 1% , 2%), and $x = 2\%$ after post-sintering in N₂ ceramics.

FIG. 3. Surface morphologies of (Mn_{0.5}Nb_{0.5})_xTi_{1-x}O₂ ceramics with doping contents of $x = 0\%$ (a), 0.25% (b), 1% (c), 2% (d), 1% after post-sintering (e), 2% after post-sintering (f).

FIG. 4. Elements mapping of $x = 2\%$ doped ceramics before (A) and after (B) post-sintering: (a) O, (b) Zr, (c) Nb, and (d) Ti.

FIG. 5. Frequency-dependence (room temperature) of dielectric properties for pure TiO₂, 1% only Nb-doped TiO₂, (Mn_{0.5}Nb_{0.5})_xTi_{1-x}O₂ ($x = 0.25\%$, 0.5% , 1% , 2%), and $x = 2\%$ after post-sintering ceramics. The logarithmic coordinates of the loss is present in the inset.

FIG. 6. Valence states of the O and Ti elements in Nb-doped TiO₂, and $x = 2\%$ doped sample before and after post-sintering: O 1s (a, b, c), Ti 2p (d, e, f).

FIG. 7. Complex impedance plots [$Z'(\omega)$ - $Z''(\omega)$] of $x = 2\%$ doped TiO₂ before (A) and after (C) post-sintering, measured from 170 °C to 380 °C. The active energy (E_a) for $x = 2\%$ doped TiO₂ before (B) after (D) post-sintering, fitted (solid lines) by Arrhenius law.

FIG.1

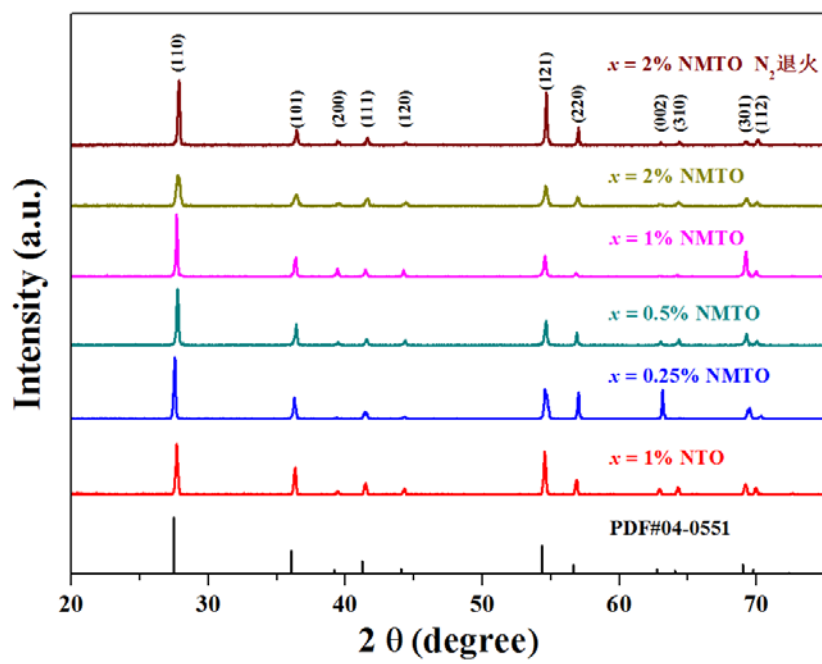


FIG.2

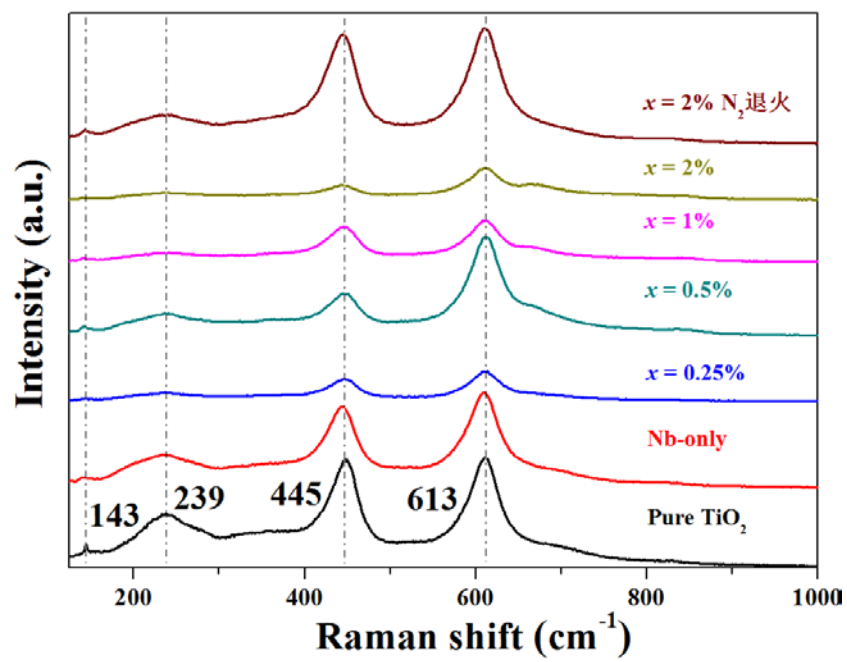


FIG.3

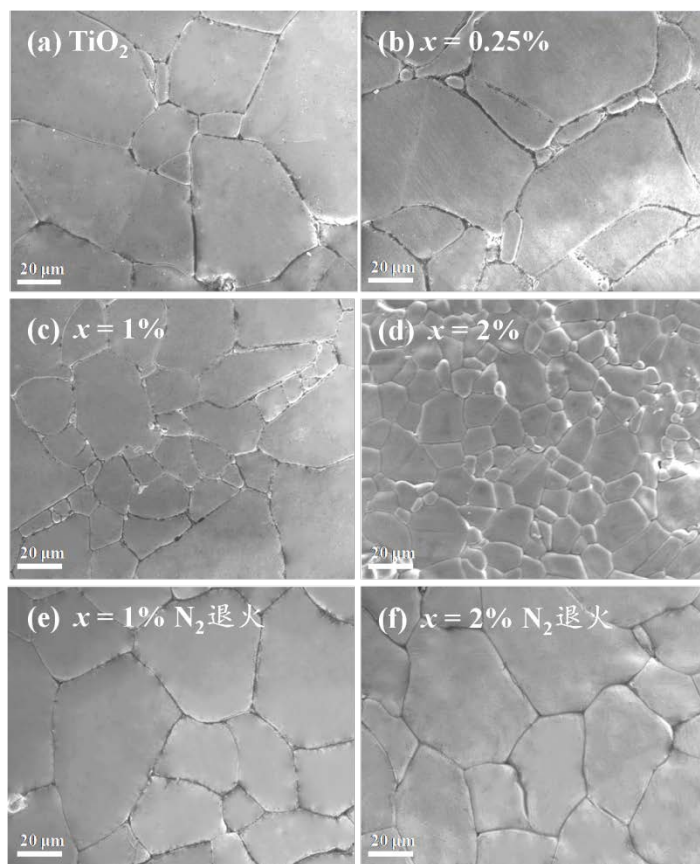


FIG.4

(A) $x = 2\%$

(B) $x = 2\%$ N₂ 退火

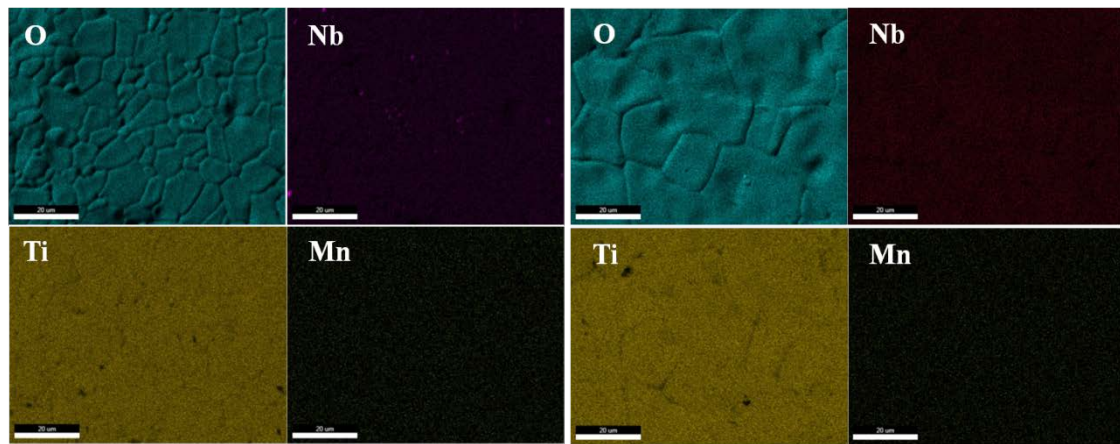


FIG.5

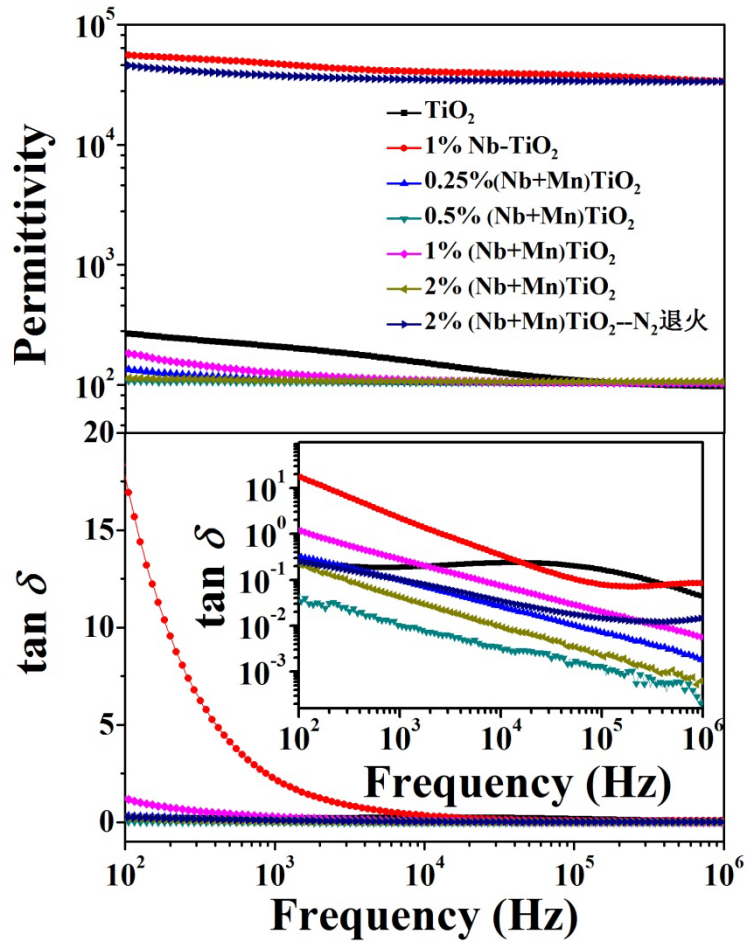


FIG.6

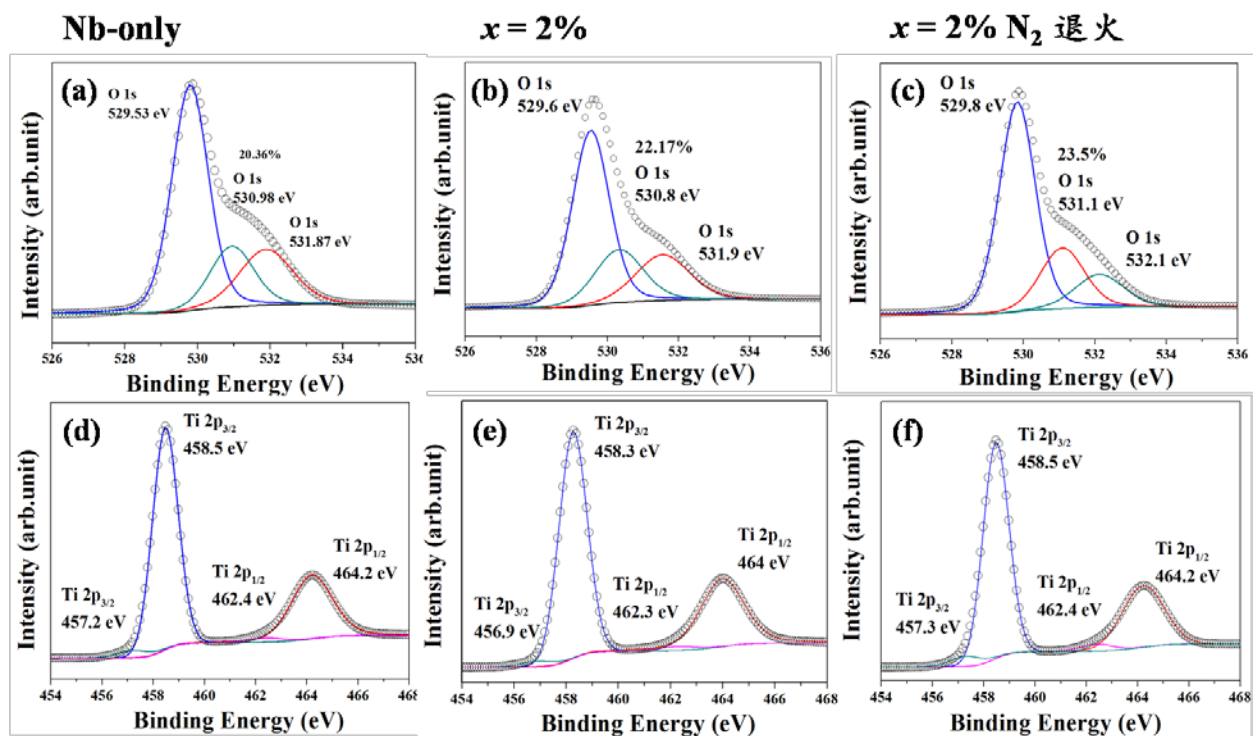


FIG.7

